Shoreline and Land Use Land Cover Changes along the 2004 tsunami-affected South Andaman Coast: Understanding Changing Hazard Susceptibility

Vikas Ghadamode[1,2], Aruna Kumari Kondarathi [1], Anand K Pandey[1,2,§] Kirti Srivastava[1]

1. CSIR- National Geophysical Research Institute, Hyderabad, 500007 India.

2. Academy of Scientific and Innovative Research (AcSIR), Ghaziabad 201002, India.

§ Corresponding author: Email address: akpandey@ngri.res.in

Tel: +91-40-27012416

Abstract

The 2004 tsunami affected the South Andaman coast, experiencing dynamic changes in the coastal geomorphology, making the region vulnerable. We focus on pre-and post-tsunami shoreline and Land Use Land Cover changes for 2004, 2005, and 2022 to analyse the dynamic change in hazard. We used GEBCO bathymetry data to calculate Run-up (m), arrival times (Min), and inundation (m) at a few locations using three tsunamigenic earthquake source parameters, namely the 2004-Sumatra, 1941-North Andaman, and 1881-Car Nicobar earthquakes. The Digital Shoreline Analysis System is used for the shoreline change estimates. The Landsat data is used to calculate shoreline and Land Use Land Cover (LULC) change in five classes, namely Built-Up Areas, Forests, Inundation areas, Croplands, and water bodies during the above period. We examine the correlation between the LULC changes and the dynamic change in shoreline due to population flux, infrastructural growth, and Gross State Domestic Product growth. India industry estimates the Andaman & Nicobar Islands losses exceed INR 10 billion during 2004, which would see a five-fold increase in economic loss due to a doubling of built-up area, a three-fold increase in tourist inflow, and a population density growth. The unsustainable decline in the forest cover, mangroves, and cropland would affect sustainability during a disaster despite coastal safety measures.

Keywords: Geomorphology, Land use Land cover, Shoreline, Tsunami, Remote sensing

1. Introduction:

The Coastal shorelines are dynamic and highly vulnerable to erosion and accretion caused by hydrodynamic, tectonic, geomorphic, and climate forcing, including tsunamis, cyclones, flooding, storm surges, wave action, wind and tide changes, and sea level variations (Nayak 2002; Boak &Turner 2005; Kumar et al., 2010; Mukhopadhyay et al., 2011). In addition to natural coastal processes, coastal resources are constantly under stress due to anthropogenic activities, such as industrialization, port construction, beach sand mining, garbage dumping, urbanization, trade, tourism, and recreational activities, which significantly impact the shoreline and results into damage to natural ecosystems (Yi et al., 2018; Davis, 2019). It is important to regularly monitor spatiotemporal along shorelines, Land use / Land Cover (LULC), and geomorphic features (Moran, 2003; Cooper et al., 2004; Scheffers et al., 2005; Jayakumar & Malarvannan, 2016). Several studies have analyzed various coastal processes, including mapping shoreline change, LULC change detection, and analysis of geomorphological landforms using satellite data. The temporal multispectral satellite data allow for the identification of regions undergoing erosion or accretion change (Misra and Balaji, 2015; Kumari et al., 2012; Tonisso et al., 2012; Murali et al., 2013; Sudha Rani et al., 2015; Rowland et al., 2022; Thiéblemont et al., 2021). The M 9.3 undersea earthquake on December 26, 2004, near the coast of Sumatra, Indonesia, triggered the Indian Ocean tsunami and caused massive destruction of the coastal ecosystem in the Andaman region (Sheth et al., 2006; Ramalanjaona, 2011). Several researchers analyzed shoreline and geomorphological changes of the 2004 Sumatra tsunami using remote sensing data (Kumari et al., 2012; Yuvaraj et al., 2014; Yunus and Narayana, 2015; Yunus et al., 2016).

Since the 2004 tsunami, the Andaman and Nicobar Islands have experienced notable population growth, infrastructural development, and flourishing tourism activities over the past decade (Yuvaraj et al., 2014). The development is profound in the south Andaman region. This

Deleted: The

Deleted: were analyzed

Deleted: statistical techniques on

is a cause of concern for the tsunami vulnerability as the region is prone to large earthquakes and is a seismo-tectonically active plate boundary. In this study, we Compute Tsunami arrival times, run-up heights, and inundation extent along the south Andaman region. We also analyzed dynamic vulnerability using temporal and spatial changes in shoreline and LULC for the tsunami-affected areas (Velmurugan et al., 2006; Ghadamode et al., 2022). The analysis covers three time periods: 2004 (pre-tsunami), 2005 (post-tsunami), and 2022 (current state) of shoreline changes using multi-temporal Landsat data employing the End Point Rate (EPR) and Net Shoreline Movement (NSM) methods (Himmelstoss et al., 2021) and LULC changes. A relationship between LULC changes and vital socioeconomic factors such as population dynamics, tourism trends, and the Gross State Domestic Product (GSDP) is established to assess the potential future impacts of tsunamis in the region. The results would provide actionable insights to the policymakers, coastal planners, and stakeholders in disaster management and sustainable coastal development.

2. Study Area

South Andaman region, with ~1,262 km² area and a 413 km coastline, is the southernmost island of the Great Andaman, where most of the Andaman Island's population and infrastructure are centered. As per the 2011 Indian census, South Andaman has a population of 238,142 people, which increased to 266,900 in 2021 (estimate based on www.census2011.co.in). The most habitable areas in the eastern part of South Andaman are located on low lands at bay heads in addition to the higher slopes bordering bays and coastal flat lands (Ghosh et al., 2004), which experienced devastation and losses during the 2004 Tsunami (Fig. 1). We selected 13 locations, namely South Point in Port Blair, Rutland Island, Corbyn's Cove Beach, Madhuban Bay, Brichgunj, Chidiyatopu, Thirupatti Temple, Wandoorjetty, Bamboo Flat, Potatang, Shoal Bay, Radha Nagar, and Govinda Nagar (Fig. 1) for vulnerability assessment in the present study.

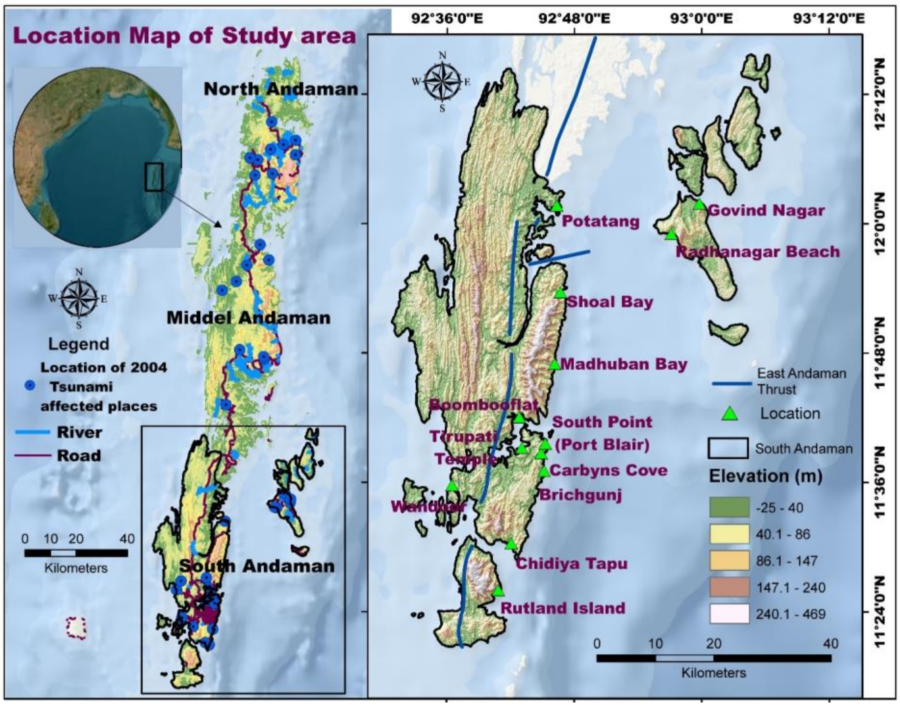

Figure 1 Location Map of the South Andaman Region (© Google Maps & © Google Earth*).*

The tectonic activity and weathering processes have influenced the region's topography growth and evolution (Curray, 2005; Bandopadhyay and Carter, 2017). The East Andaman Thrust, also called East Boundary Thrust, is a linear/curvilinear ~500 km long fault zone and is the locus of ongoing convergent and crustal deformation along the Sunda-Andaman plate boundary. This structure is pivotal in creating accretionary prisms within the outer-arc ridge of the Andaman and Nicobar subduction zones (Fig. 1; Bhat et al., 2023).

The structure-bound major geomorphological features in South Andaman include hills, valleys, beaches, mangroves, and coral reefs (Fig. 2a). The highest peak on the island is Mount Harriet, with approximately 1,200 m (3,937 feet) (southandaman.nic.in). The north-western and north-eastern parts of South Andaman are highly and moderately dissected, whereas the Southern part has low dissected structural hills and valleys (Fig. 2a, b, c, and d). The upper slopes of the region are covered with high dissected structural hills with dense pristine forest (Fig. 2a). The slope ranges between 0 to 44.9 degrees, with lower slopes in the coastal region mostly inhibited and undergoing rapid coastline modification and Land Use Change. The North, Northeast, and Southern portions of South Andaman have the steepest slope and relief area, while the Eastern, Southeastern, and western parts have relatively lower slopes (Fig. 2b and c). The island has a rough coastline with various bays, inlets, and headlands (Fig. 2). The Younger coastal plain is a relatively flat and low-lying area adjacent to the coastline, which is formed through the accumulation of sediments brought by the ocean (Fig. 2e). A wave-cut platform, formed by the erosive action of waves, are flat or gently sloping rock surface are found along South Point coastlines in Port Blair (Fig. 2f). These platforms can be exposed at low tide, which gradually wear away the rock over time, are unique feature of rocky coastlines. Coral reefs along the coast contribute to the formation of sandy beaches and barrier islands (Reguero et al., 2018). Mangrove forests are found on coasts in South Andaman Island, primarily in the salty water and muddy sediments lagoons and tidal zone (Fig. 2g). Mangroves are crucial in stabilizing coastal ecosystems and providing habitat for various species. Wandoor, Chidya tapu, and Sippighat are some notable locations of mangrove forests in South Andaman coastal areas. The coastal plains in south Andaman are dynamic and prone to tsunamis due to their location and active plate boundary. Therefore, studying shoreline change and LULC change is especially important because of the potential impacts on local communities and ecosystems.

Deleted: forming

Deleted: brackish

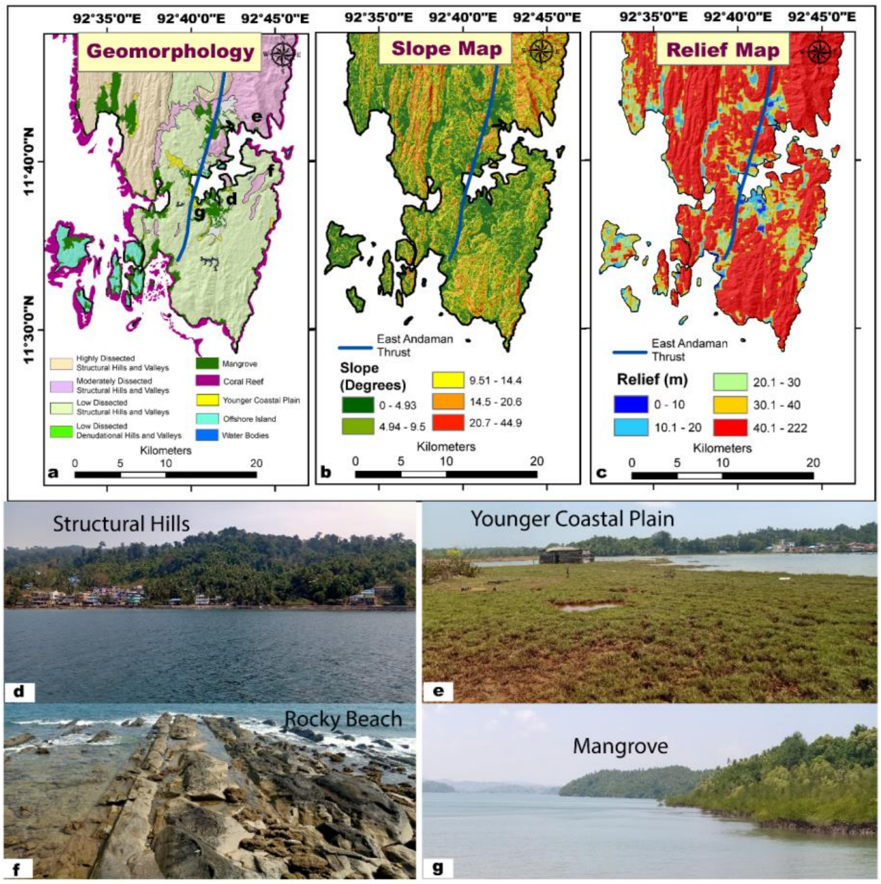

Figure 2 (a) *Geomorphology,* ***(b)*** *Slope map,* ***(c)*** *Relief Map,* ***(d)*** *Structural Hills,* ***(e)*** *the younger coastal plain,* ***(f)*** *Rocky Beach with a wave-cut platform near south point, Port Blair,* ***(g)*** *Mangrove.*

3. Materials and Methods

It is imperative to generate a spatial dataset that may have a bearing on the dynamic changes to assess the vulnerability.

3.1 Data Used

Landsat satellite data, such as Thematic Mapper (TM) and Operational Land Imagery (OLI) sensor for the years 2004, 2005, and 2022, is used to analyze shoreline and monitor the LULC changes along the South Andaman coast in the present study. The Shuttle Radar

Topography Mission (SRTM) Digital Elevation Model (DEM) is used to prepare the study area's slope and relief map. We used the General Bathymetry Chart of the Ocean (GEBCO) for run-up and inundation studies along the south Andaman coastal areas (Table 1).

Table 1: Data used in the present study region

Data	Purpose	Date & Year	Resolution	Sources
GEBCO bathymetry	Inundation and Run-Up	2022	90 m	GEBCO (https://www.gebco.net/)
Landsat 5 TM, Landsat 8 OLI	LULC and Shoreline Change Analysis	26-02-2004 27-01-2005 27-02-2022	30 m	USGS Earth Explorer
SRTM DEM	Slope, Relief	-	30m	USGS Earth Explorer
Geomorphology	Geomorphology	-	1:250k	bhukosh.gsi.gov.in
Socioeconomic data	Population, Tourism, Gross State Domestic Product (GSDP)	1991-2021 2001-2020	-	(censusindia.gov.in) (Directorate of economics and statistics) (Rbi.org.in)

3.2 Tsunami Modeling

Several attempts have been made to model tsunamis to calculate inundation and determine run-up heights to evaluate their impact and hazards along mainland Indian coastal areas and elsewhere (Cho et al, 2008; Srivastava et al., 2021; Sugawara, 2021; Dani et al. 2023).

3.2.1 Tsunamigenic source

Mansinha and Smyile (1971) and Okada (1985) derived closed-form expressions for the stress and strain field at the source location for different source mechanisms. The focal mechanism and fault parameters like strike angle, dip angle, slip, and focal depth are necessary to compute the initial deformation at the source at t=0 sec (Ioualalen (2007), Rani et al. (2011), Mishra et al. (2014), and Srivastava et al. (2021)). The December 26, 2004, Sumatra earthquake of magnitude 9.3 had ruptured almost 1400 km. The region is known to have ruptured into five segments with different slip distributions. Other great tsunamigenic earthquakes in the

Deleted: Run-ups and Inundation

Deleted: (Rani

Deleted: ., 2011

Deleted:). However, despite experiencing historical tsunamis during the 31

Deleted: ,

Andaman region are the 1881-Car Nicobar and the 26 June, 1941-North Andaman earthquakes (Table 2).

Table 2: Tsunamigenic earthquake deformation parameters used to simulate different scenarios a) 1881-Car Nicobar, and b) 1941-North Andaman earthquakes (Mishra et al., 2014), and c) 2004-Sumatra (Ioualalen, 2007).

	1881-Car Nicobar	1941 -North Andaman	2004 Sumatra Earthquake				
Input Parameters			Seg1	Seg2	Seg3	Seg 4	Seg5
Longitude (DD)	92.43	92.5	94.57	93.90	93.21	92.60	92.87
Latitude (DD)	8.52	12.1	3.83	5.22	7.41	9.70	11.70
Focal Depth (km)	15	30	25	25	25	25	25
Strike angle (°)	350	20	323	348	338	356	10
Rake (°)	90	90	90	90	90	90	90
Slip (m)	5	5	18	23	12	12	12
Fault Length (km)	200	200	220	150	390	150	350
Fault Width (km)	80	80	130	130	125	95	95
Dip (°)	25	20	12	12	12	12	12
Magnitude (Mw)	7.9	7.7	9.3				

3.2.2 Tsunami wave propagation

The Tohoku University's Numerical Analysis Model for the Investigation of Near field tsunamis (TUNAMI-N2) to simulate the tsunami run-ups and impact using explicit leap-frog finite-difference methods by solving nonlinear shallow water wave equations, incorporating bathymetry, earthquake source parameters, and fault geometry (Imamura and Imteaz, 1995; Imamura, 1996; Goto, 1996; Imamura et al., 2006; Yalciner et al., 2003). The 2-dimensional governing equations for tsunami modeling are:

$$\frac{\partial \eta}{\partial t} + \frac{\partial M}{\partial x} + \frac{\partial N}{\partial y} = 0$$

$$\frac{\partial M}{\partial t} + \frac{\partial}{\partial x}\left(\frac{M^2}{D}\right) + \frac{\partial}{\partial y}\left(\frac{MN}{D}\right) + gD\frac{\partial \eta}{\partial x} + \frac{gn^2}{D^{7/3}} M\sqrt{M^2 + N^2} = 0$$

Deleted: ,

Deleted: , and the 26 December, 2004-Sumatra earthquakes, the south Andaman region is yet to be explored for scenario hazard assessment. We

Moved (insertion) [1]

Moved (insertion) [2]

Deleted: the

Deleted: to solve

Deleted:).

$$\frac{\partial N}{\partial t}+\frac{\partial}{\partial x}\left(\frac{MN}{D}\right)+\frac{\partial}{\partial y}\left(\frac{N^2}{D}\right)+gD\frac{\partial \eta}{\partial y}+\frac{gn^2}{D^{7/3}}N\sqrt{M^2+N^2}=0 \qquad (1)$$

In the equation-1, D is the total water depth given by h+η, τ_x, and τ_y the bottom frictions in the x- and y- directions, A the horizontal eddy viscosity which is a constant in space, and the shear stress on a surface wave is neglected. M and N are the discharge fluxes in the x- and y- directions which are given by

$$M=\int_{-h}^{\eta} u dz = u(h+\eta) = uD \qquad N=\int_{-h}^{\eta} v dz = v(h+\eta) = vD \qquad (2)$$

The bottom friction is generally expressed as follows

$$\frac{\tau_x}{\rho}=\frac{1}{2g}\frac{f}{D^2}M\sqrt{(M^2+N^2)} \qquad \frac{\tau_y}{\rho}=\frac{1}{2g}\frac{f}{D^2}N\sqrt{(M^2+N^2)} \qquad (3)$$

The friction coefficient ‘f’ and Manning's roughness ‘n’ are related by

$$n=\sqrt{\frac{fD^{1/3}}{2g}} \qquad (4)$$

It is seen that when D is small and f becomes large then n remains almost a constant. Substituting M, N, and the above values in fundamental equations of TUNAMI N2 are obtained which are used to solve the wave propagation using the explicit Leap-Frog finite difference Scheme as Given by Imamura, (2006).

3.2.3 Computational grid

In deep-sea regions with longer wavelengths, a coarse grid spacing to model linear effects is sufficient to resolve the wave with minimal error. As the tsunami wave propagates from deep to shallow waters, the wavelength shortens and the amplitude increases, it follows a non-linear pattern of amplitude dispersion, energy dissipation, and bottom friction and requires finer resolution grids with more node points to accurately capture the wave dynamics and minimize errors. The grid spacing should follow the Courant-Friedrich-Lewy conditions for checking the

Deleted: where

Deleted: follow

Deleted: require

convergence of the numerical code to a certain asymptotic limit using the following relationship,

$$\Delta x/\Delta t = \sqrt{(2gh_{max})} \qquad (5)$$

Where Δt and Δx are temporal and spatial grid sizes, hmax maximum still water depth in the computational domain, and g is the gravitational acceleration.

To observe the non-linear or near-shore effects of a tsunami a high-resolution bathymetry and topography is considered. In the present study, we used GEBCO bathymetry and topography data formatted into four grids of 81, 27, 9, and 3arc seconds resolutions at a spacing ratio of 1:3 for grids A, B, C, and D, respectively (Fig. S1). In most computations, the manning coefficient is around 0.025 as it consists of gravel and sand (Masaya et al., 2020); however, different manning coefficients can be considered for rough bathymetry (Dao and Tkalich, 2007). A value of 0.01 is considered for smooth bathymetry and stony cobbles, and a roughness of 0.035 can be considered. The viscosity and roughness have a certain influence on mild slopes but it is negligible for steep slopes and a dynamic friction coefficient from 0.01 to 0.1 can be considered (Zhang et al., 2024). For the propagation of tsunamis in shallow water, the horizontal eddy turbulence terms are negligible as compared with the bottom friction (Dao and Tkalich, 2007) We simulate the tsunami waves using the TUNAMI-N2 code to get the directivity map, the wave amplitudes (run-up heights), and inundation distance at different locations in the study region.

3.3 Shoreline Analysis in DSAS

The USGS's digital shoreline analysis system (DSAS) version 5.1 (an ArcGIS extension) estimates shoreline changes. The procedures are executed in 4 steps: shoreline digitization, baseline generation, transect generation, and computation of the shoreline change rate (Raj et al., 2020; Natarajan et al., 2021). The digitized shorelines for 2004, 2005, and 2022

Deleted: Based on above conditions we used GEBCO bathymetry and topography data formatted into four grid of 81, 27, 9 and 3arc seconds resolutions at spacing ratio of 1:3 for grids A, B, C, and D, respectively.

Deleted: The TUNAMI-N2 code uses Mansinha and Smyile's (1971) deformation model to estimate

Deleted: seafloor upliftment

Deleted: source

Deleted: the focal mechanism solutions

Deleted: fault parameters are necessary to compute the initial deformation at the source at t=0

Deleted: . In addition to the grid resolution, the calibration requires earthquake source parameters (e.g., slip distribution, fault length

Deleted: width), which we adopted based

Deleted: Ioualalen (2007), Rani et al. (2011), Mishra

Deleted: . (2014), and Srivastava et al. (2021) (Table 2). The five segments

Deleted: different slip distributions of Sumatra earthquake (December 26, 2004) with ~1400 km rupture length (Ioualalen

Deleted: are considered for modeling. We run

Deleted: with above input parameters

Deleted:)

Deleted: tide-gauge

Deleted: **Table 2** Tsunamigenic earthquake deformation parameters used to simulate different scenarios a) 1881-Car Nicobar, and b) 1941-North Andaman earthquakes (Mishra et al.,

Moved up [1]: 2014), and c) 2004-Sumatra (Ioualalen, 2007).

Moved up [2]: ¶
1881-Car Nicobar

years have been added to a personal geodatabase in a single shapefile. The shoreline image data is added to the attributes as MM/DD/YYYY, and the baseline is in the meter UTM projected coordinate system. To estimate rates of change, DSAS uses baseline measurements of a time series of shorelines and a shapefile (Leatherman, 2003). Generating transects involves initially choosing a predefined set of parameters from the personal geodatabase, including settings for the baseline and shoreline. Subsequently, we placed these transects perpendicular to the shoreline, extending 800 m at intervals of 150 m along the entire shoreline, originating from the baseline. A 50 m smoothing distance was applied using the 'cast transects' tool within DSAS to ensure a smoother outcome.

The evaluation of uncertainty encompasses natural and anthropogenic forces such as wind, waves, tides, currents, and human influences, along with the accuracy of measurement techniques, including digitization, interpretation, and GPS error. The accuracy of shoreline position and the rates of shoreline change can be influenced by various error sources, such as the position of the tidal level, image resolution, digitization error, and image registration (Jayson-Quashigah et al., 2013; Vu et al., 2020, Basheer et al., 2022). Therefore, the shoreline positional error (Ea) for each transect was calculated using Equation (6):

$$E_s = \pm\sqrt{E_s^2 + E_w^2 + E_d^2 + E_r^2 + E_p^2} \quad (6)$$

Where Es is the seasonal error due to seasonal shoreline fluctuations, which is ~ +5 m in extreme ocean level (EOL); Ew is the tidal error, Ed is the digitization error, E_r is the rectification error and E_p is the pixel error (Fletcher et al. 2011; Vu et al., 2021). This approach assumes that the component errors are normally distributed (Dar & Dar, 2009). The total uncertainties were used as weights in the shoreline change calculations. The values were annualized to provide errors (E_u) estimation for the shoreline change rate at any given transect, expressed in Equation (7):

$$E_u = \pm \frac{\sqrt{U_{t1}^2 + U_{t2}^2 + U_{t3}^2 + U_{t4}^2 + U_{tn}^2}}{T} \quad (7)$$

where t_1, t_2, and tn are the total shoreline position error for the various years and T is the years of analysis.

The uncertainty in the shoreline analysis is due to the influence of tides on the Landsat satellite imagery, which is minuscule in the extensive coastline of the study area. We used monthly tide gauge data from the Permanent Service for Mean Sea Level (PSMSL) database (https://psmsl.org/data/obtaining/stations/206.php) at Port Blair station for 2003-2004 and 2017-2021. The data for 2004-2005 and 2022 are unavailable. The tide excursion of 383 mm or 0.383 m (Fig. S2) is estimated from the highest (1100 mm) and lowest (717 mm) tide gauge measurements recorded between 2017 and 2020. We calculated uncertainty of 7.21m and 7.12m for 2018-2019 and 2019-2020, respectively, and the same is adopted for 2022 owing to similar ranges (Table S1). The mean slope of the shore areas is 4-12 degrees near 7 zones. (Fig. S3, Table S2). We used End Point Rate (EPR) and Net Shoreline Movement (NSM) methods to analyze the shoreline change (Himmelstoss et al., 2021). To quantify uncertainty, a confidence interval of 90% and a shoreline uncertainty value of 10m were adopted based on the recommendations of the United States Geological Survey (USGS) under the National Assessment of Shoreline Change project (Himmelstoss et al., 2021; Den and Oele, 2018 and Joesidawati, 2016).

3.3.1 Net Shoreline Movement (NSM)

NSM is used to determine the net change in the shoreline position over a specific period by finding the perpendicular distance between the most recent shoreline (in this case, 2022) and the oldest shoreline (2004) along each transect. The formula for NSM can be expressed as:

Deleted: The

Deleted: of Port Blair station for 2004-2005 and 2022 are unavailable in

Deleted:). We calculated uncertainty of 7.46m and 7.13m

Deleted: .

Deleted: we have adopted

Deleted: assigned

Deleted: 10 meters as per

Deleted: We used End Point Rate (EPR) and Net Shoreline Movement (NSM) methods to analyze the shoreline change. The statistical mean of these parameters was computed using USGS's DSAS tool (Himmelstoss et al., 2021).

Deleted: a statistical parameter

$$NSM = \{d_{2022} - d_{2004}\} m$$

3.3.2 End Point Rate (EPR)

EPR quantifies the shoreline change rate over time and is calculated by dividing the Net Shoreline Movement (NSM) by the time elapsed between the oldest and most recent shoreline measurements, which indicates the rate of erosion or accretion. It is important to have data from at least two shoreline dates (Dolan et al., 1991; Crowell et al., 1997). The formula for EPR can be expressed as follows:

$$EPR = \left\{ \frac{d2022 - d2004}{t2022 - t2004} \right\}$$

3.4 Land Use Land Cover Analysis (LULC)

The LULC map uses Landsat 5 TM (2004 and 2005) and Landsat 8 OLI (2022). False Colour Composite (FCC) satellite images combine near-infrared, red, and green bands to delineate five classes: Forest, built-up, Cropland, Water bodies, and Inundated areas. (Prabhbir and Kamlesh, 2011). Tone, texture, size, shape, pattern, association, and other visual interpretation techniques also were used to interpret different land use classes. Maximum likelihood is a supervised classification method used in this study to detect LULC change. Each pixel in the classified Landsat images varies over time due to changes in land cover.

4. Results

An analysis of the 2004 tsunamigenic earthquake's impact on the South Andaman region, focusing on tsunami directivity, arrival times, run-up heights, shoreline changes, and LULC impact, is examined in detail.

4.1 Tsunami studies along the South Andaman Region

We have considered three tsunamigenic seismic scenarios, namely, a) the 1881-Car Nicobar earthquake, b) the 1941-North Andaman earthquake, and c) the 2004 Sumatra earthquake, and generated the directivity and run-up maps(Fig. 3). The directivity map shows

Deleted: is a statistical parameter quantifying

Deleted: model

that most of the energy propagation is in the East-West direction (Fig. 3 a,b,c), and the shallower waters surrounding the Andaman and Nicobar Islands has significance influence on the east-west propagation of tsunamis (Singh et al., 2012). The run-up height along the eastern coast of South Andaman is greater than the western coast (Fig. 3 b', c', d'; Table 3). This difference is due to the wider continental shelf on the Western coast of the south Andaman region and shallow water depths. In the case of a higher magnitude of tsunamigenic earthquakes in the Car Nicobar or the North Andaman region, higher run-ups will be observed along the locations, which are considered for the present study (Table 3).

Deleted: gauge

The arrival times of tsunamis vary from 21 minutes to 58 minutes across different locations for these earthquakes, with the 1881-Car Nicobar earthquake generally resulting in the shortest arrival time (Fig. 3; Table 3). The run-up heights range from 1-13 m at different locations (Fig. 3; Table 3), which are resultant of earthquake magnitude, the source's proximity to observation locations, and the local coastal topography that also affected inundations. The extent of inundation, representing the area covered by the tsunami, ranges from 10m to 950m, with a wide variation across locations and earthquake events. The 2004 Andaman Sumatra earthquake resulted in higher run-up heights and inundations compared to the 1881 Car Nicobar, and 1941 Andaman earthquakes and caused extensive damage. Hence, we considered the 2004-Andaman Sumatra earthquake for a detailed analysis of hazard assessment and scenario analysis. The arrival times (minutes), run-up height (meter), and inundation extent (meter) at 13 different locations along the South Andaman region for the 2004 Sumatra earthquake (Table 3) are considered for further analysis.

Deleted: .75

Deleted: were influenced by

Deleted: Therefore

Deleted: Minutes

Deleted: Inundation

Deleted: by

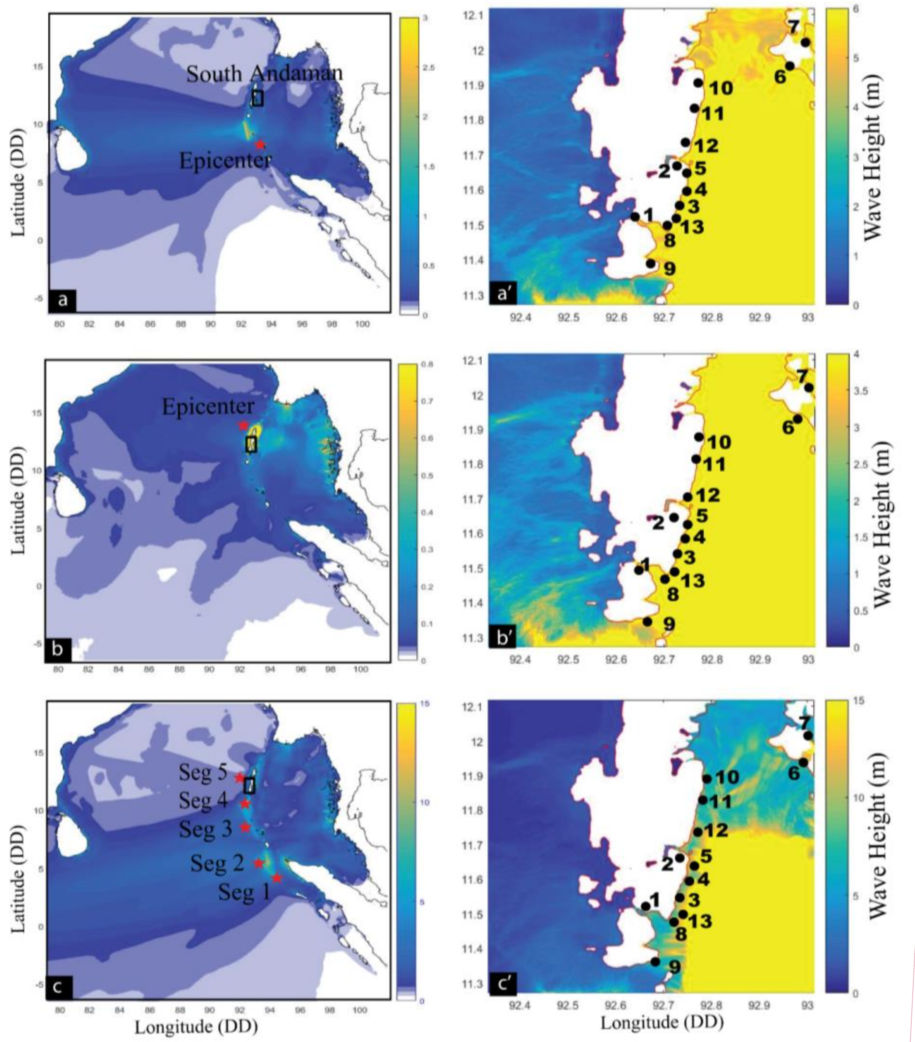

Deleted:

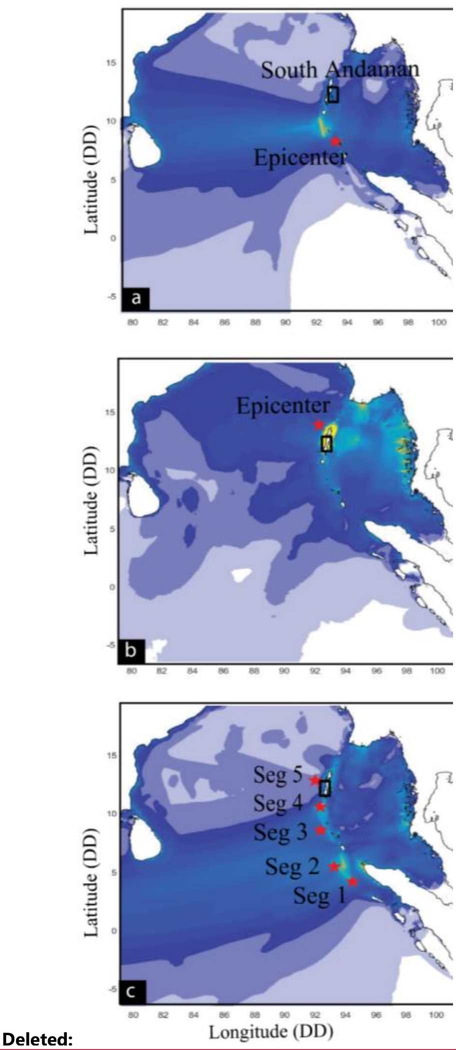

*Figure 3: (a) Directivity and (a') wave run-up height for the 1881-Car Nicobar, (**b** and **b'**) for the 1941-Andaman, and (c and c') for the 2004-Sumatra earthquakes.*

Table 3: Estimated Arrival times, Run-up heights, and inundations at the studied locations from tsunamigenic a) 1881-Car Nicobar, b)1941-North Andaman earthquakes, and c) 2004-Sumatra earthquake sources. The SN of locations is common for Figs. 3 and 4.

SN	Gauge Locations	Longitude Latitude (DD)	Earthquake Sources	Arrival Time (Min.)	Run-up (m)	Inundation (m)
1	Wandoorjetty	92.614750, 11.581667	a) 1941-North Andaman	22.5	1.25	180
			b) 1881 Car Nicobar	32.80	2.21	200
			c) 2004 - Sumatra	***36.5***	***3.5***	***450***
2	Bombooflat	92.715417, 11.700722	a) 1941-North Andaman	24.55	2.23	350
			b) 1881 Car Nicobar	31.2	2.35	650
			c) 2004 - Sumatra	***42***	***5.5***	***90***
3	Corbyns Cove Beach	92.770916, 11.642372	a) 1941-North Andaman	22.3	2.1	320
			b) 1881 Car Nicobar	28.8	2.3	580
			c) 2004 - Sumatra	***33***	***12.7***	***900***
4	South Point, Port Blair	92.702917, 11.652389	a) 1941-North Andaman	22	2.12	280
			b) 1881 Car Nicobar	28.4	2.31	500
			c) 2004 - Sumatra	***31.5***	***9.6***	***550***
5	Thirupatti Temple	92.703861, 11.581694	a) 1941-North Andaman	21.75	1.42	360
			b) 1881 Car Nicobar	46.5	1.65	400
			c) 2004 - Sumatra	***38***	***1***	***200***
6	Radha Nagar	92.951722, 11.979306	a) 1941-North Andaman	52	2.1	180
			b) 1881 Car Nicobar	54	3.8	220
			c) 2004 - Sumatra	***54***	***2.6***	***156***
7	Govinda Nagar	92.989139, 12.030167	a) 1941-North Andaman	56	1.8	220
			b) 1881 Car Nicobar	58	3.2	190
			c) 2004 - Sumatra	***58***	***3.6***	***195***
8	Chidiyatopu	92.716639, 11.499306	a) 1941-North Andaman	21.75	1.79	300
			b) 1881 Car Nicobar	26.5	2.05	500
			c) 2004 - Sumatra	***36***	***3.9***	***585***
9	Rutland Island	92.703818, 11.431497	a) 1941-North Andaman	25.9	1.01	585
			b) 1881 Car Nicobar	26.55	1.44	380
			c) 2004 - Sumatra	***27***	***6***	***700***
10	Shoal Bay	92.795963, 11.934202	a) 1941-North Andaman	34.8	1.77	180
			b) 1881 Car Nicobar	42.5	1.45	220
			c) 2004 - Sumatra	***56***	***13***	***950***
11	Potatang	92.801282, 12.027380	a) 1941-North Andaman	36	1.5	200
			b) 1881 Car Nicobar	46	1.4	180
			c) 2004 - Sumatra	***58***	***12.5***	***210***
12	Madhuban Bay	92.785534, 11.782775	a) 1941-North Andaman	32	1.9	180
			b) 1881 Car Nicobar	40	1.5	200
			c) 2004 - Sumatra	***54***	***6.9***	***210***
13	Brichgunj	92.770162, 11.618980	a) 1941-North Andaman	28	1.3	200
			b) 1881 Car Nicobar	32	4	300
			c) 2004 - Sumatra	***30***	***10***	***585***

Due to the effects of the 2004 tsunami, the stagnation of tsunami water in the agricultural lands and low-lying areas of the Wandoor region resulted in increased soil salinity (Fig. 4a); it also damaged the bridge in the Bombooflat area (Fig. 4b), and houses near the Sippighat area (Fig. 4c, d). Shoal Bay recorded the highest inundation extent of 950m and experienced the highest run-up height of 13m, indicating significant wave impact (Fig. 3b; Table 3). Corbyn's Cove Beach and Rutland Island experienced significant inundation distances exceeding 700m (Fig.3b, Table 3). Potatang, Corbyns Cove Beach, and Brichgunj also recorded relatively high run-up heights that exceeded 9m (Table 3). Most locations experienced arrival times between 27 and 58 minutes, indicating a relatively quick propagation of the tsunami wave. Jain et al. (2005) mentioned that tsunami waves arrived between 40 and 50 minutes in the Andaman and Nicobar Islands. Our results agree with the tsunami run-up heights estimation by Cho et al. (2008) and Prerna et al. (2015) at a few locations in the present study area. Since the tide gauge data are available at a few locations along the Indian coast, we rely on limited field observations along the coast to validate our findings. The field observations of the water marks on a light post at Bambooflat in Port Blair. was seen to be around 3.8m (Cho et al., 2008) and our computations show it to be ~ 3.5m, which is within ~7% error limit. Similarly at South Point, Port Blair, the field observations are 10m, and our computations value is 9.6m, which is ~4% deviation and the deviation is 7% at Chidiyatopu. The Bambooflat region and Harbour area of Port Blair experienced liquefaction affecting several buildings (Murty et al., 2006), our computations have shown that the tsunami wave heights were around 5.5m. At most locations, the computed values are within 10% error.

Deleted: The results show that the run-up heights range from 1 to 13 m, arrival times range from 27 to 58 min, and the inundation extent range from 90 to 950m, suggesting a significant variability in the tsunami's impact across the South Andaman Region.

Deleted: .

South Andaman experienced significant inundations during the 2004 Sumatra earthquake, highlighting the urgent need for robust mitigation and preparedness measures in these vulnerable coastal regions. We aim to contribute to this broader goal by providing essential data and insights to support evidence-based decision-making and mitigate the adverse impacts of tsunamis on coastal populations. The study will provide workable input to the local risk management strategies involving local communities, optimizing evacuation planning, enhancing early warning systems, fortifying infrastructure resilience, and adopting a multi-hazard risk assessment approach (National Research Council, 2011).

Figure 4: (a) Stagnation of Tsunami water in the agricultural field and Low-laying areas in Port Blair, (b) damaged bridge in Bombooflat, (c, d) damaged house in the Sippighat area near Port Blair (Photo: 01/03/2023). The number on the field photograph corresponds to respective locations as in Fig. 3.

4.2 Shoreline Change during Tsunami (2004-2005) and post-tsunami (2005-2022)

Deleted: 2021

The south Andaman coasts are divided into seven zones based on proximity with the inundation studies to calculate NSM and EPR to understand the short-term and long-term changes impact of coastal erosion (Fig. 5, Supplement Fig. S4-S10). The NSM and EPR are calculated over two separate time frames to comprehend the damages caused by tsunamigenic and regular wind-wave-surge events in South Andaman Island. These zones were used to understand erosion and accretion rates between (i) 2004 - 2005 (Fig. 5a) and (ii) 2005-2022 (Fig. 5b). The EPR and NSM values from 2004 to 2005 indicate the direct effect of tsunami

Deleted: S1-S7

waves, whereas 2005 to 2022 values represent periodic wind-wave-surge dynamics. Periodic coastal shoreline changes refer to the regular and repeating fluctuations in the position of the shoreline along the coast. Natural and human-induced factors can influence these changes. A total of 1,083 transects are created at 50-m intervals, distributed among the zones as follows: Zone 1 (339 transects), Zone 2 (147 transects), Zone 3 (89 transects), Zone 4 (74 transects), Zone 5 (137 transects), Zone 6 (73 transects), and Zone 7 (220 transects). The shoreline variation rates indicate positive accretion and negative erosion (Fig. 6, Table 4). The EPR Changes in meters per year (m/y) for the periods 2004-2005 show a higher erosion rate compared to 2005-2022, particularly in Zones 3, 4, and 5 (Fig. 6a). The NSM focused on two distinct time frames, indicate the NSM rates during the tsunami, for the year of 2004-2005, and the NSM rates over the extended 17-year period from 2005 to 2022 are measured in meters (Fig. 6b). The detailed analysis of the maximum (accretion), minimum (erosion), and mean shoreline changes for each of the seven zones that occurred during the tsunami event and the post-tsunami period are discussed below.

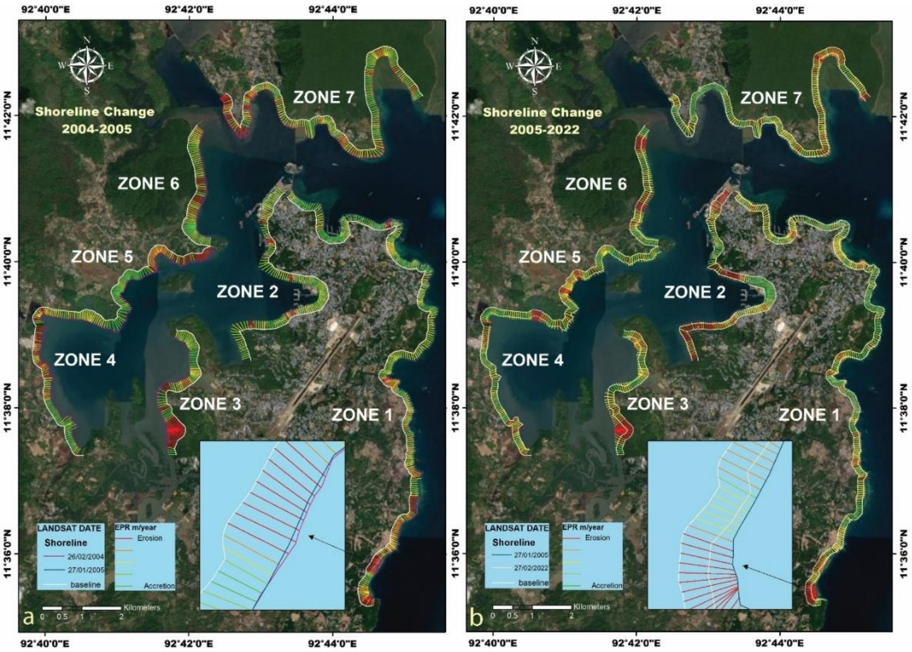

Figure 5: Shoreline changes observed (a) during 2004-05 due to the tsunamigenic process and (b) from 2005-2022 due to wind wave surges overlaid on Google Earth images (@Google Earth). The affected coastline is subdivided into seven distinct zones for detailed analysis.

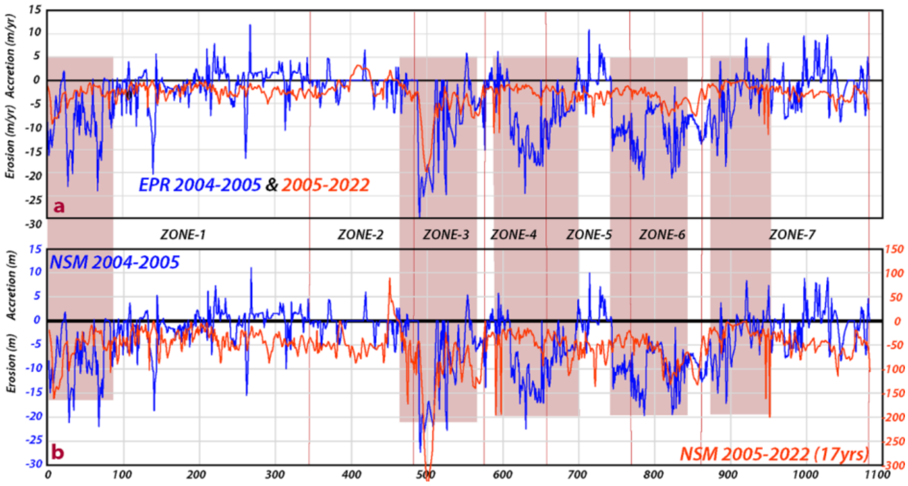

Figure 6: (a) The rates of erosion and accretion in seven distinct Zones along the South Andaman shoreline using EPR methods, and (b) NSM have been conducted between the years 2004-2005 and 2005-2022. Highlighted color indicating high erosion zone

Table 4 Shoreline change in southern Andaman is observed for 2004-2005 and 2005-2022 using USGS's DSAS methods (Himmelstoss et al., 2021).

		2004-2005		2005-2022	
ZONE		**EPR(m/y)**	**NSM(m)**	**EPR(m/y)**	**NSM (m)**
ZONE 1	Mean	-2.85	-2.62	-2.55	-43.57
	Minimum	-23.9	-21.29	-9.44	-161.21
	Maximum	12.05	11.06	0	0
ZONE 2	Mean	-0.54	-0.50	-1.0639	-18.174
	Minimum	-7.17	-6.58	-4.56	-77.93
	Maximum	6.54	6	3.25	55.56
ZONE 3	Mean	-9.92	-8.11	-7.10	-121.51
	Minimum	-24.71	-23.27	-19.87	-339.51
	Maximum	5.58	4.37	-1.02	-17.42
ZONE 4	Mean	-7.92	-7.72	-2.24	-38.34
	Minimum	-24.47	-22.46	-11.42	-195.03
	Maximum	6.23	5.72	-0.79	-13.42
ZONE 5	Mean	-6.594	-6.05	-2.94	-50.26
	Minimum	-21.47	-19.7	-7.95	-135.83
	Maximum	10.88	9.99	-1.03	-17.54
ZONE 6	Mean	-9.74	-8.94	-4.92	-84.05
	Minimum	-21.18	-19.44	-7.75	-132.39
	Maximum	-1.46	-1.34	-1.86	-31.73
ZONE 7	Mean	-2.16	-1.986	-2.43	-41.56
	Minimum	-18.65	-17.29	-11.7	-199.96
	Maximum	9.77	8.97	-0.04	-0.61

ZONE 1: This zone experienced a combination of erosion and accretion between 2004-05 and 2005-21. The maximum erosion rates are observed at Megapoda, with an EPR of -23.9 m/y. and -9.44 m/y., NSM analysis shows the estimated erosion is -21.29m and -161.21m respectively (Fig. S4 a, b, Table 4). The southern part of South Andaman Island has more shoreline erosion rather than accretion, which can be attributed to the heightened impact of tsunamis on the southern region, a phenomenon that is more significant when compared to the northern part of South Andaman Island. These Sediments eroded from one coastline area are often transported along the shoreline by the longshore currents. The angle of wave approach creates these currents and is responsible for moving sediment parallel to the coastline.

Deleted: S1

ZONE 2: This zone experienced a combination of erosion and accretion between 2004-05 and 2005-21. The maximum rate of erosion is -7.17 m/y and -4.56 m/y (EPR) was recorded at IOC Colony, while the maximum accretion rate of 6.54 m/y and 3.25 m/y (EPR) was observed at Ashwin Nagar Respectively. The NSM analysis indicated a shoreline retreat of -6.58 m at IOC Colony and -77.93 m advancement at Ashwin Nagar. The jetties in the Jungli Ghat port played a role in controlling erosion and accretion at these sites (Fig. S5, Table 4).

Deleted: S2

ZONE 3: This zone experienced a combination of erosion and accretion between 2004-05 and 2005-21. The maximum erosion rate is -24.71 m/y and -19.87 (EPR) at Flat Bay, while the maximum accretion rate is 5.58 m/y and (EPR) at NLC Limited. The NSM analysis revealed a shoreline retreat of -23.27 m and -339.51 m at Flat Bey. High wave energy and exposure to strong currents, which are more common near Flat Bay, can lead to increased erosion of mangrove shorelines (Fig. S6, Table 4).

Deleted: S3

ZONE 4: This zone experienced a combination of erosion and accretion between 2004-05 and 2005-21. The maximum erosion rate is -24.47 m/y at Ferrargunj and -11.24 m/y (EPR) at PLK Creek Resort, NSM estimated erosion is -22.46 m and -195.03m at Chouldari (Fig. S7). We observed the shoreline erosion area using the Landsat time-lapse satellite images between 2004-2005, and 2022 near Flat Bay, South Andaman, has revealed noteworthy environmental changes. The dark blue color observed in 2004 and 2005 indicates the presence of deep-water bodies, whereas the light blue color in the 2022 image suggests the water bodies have become shallow with significant fresh sediment load (Fig. 7; Table 4).

Deleted: S4

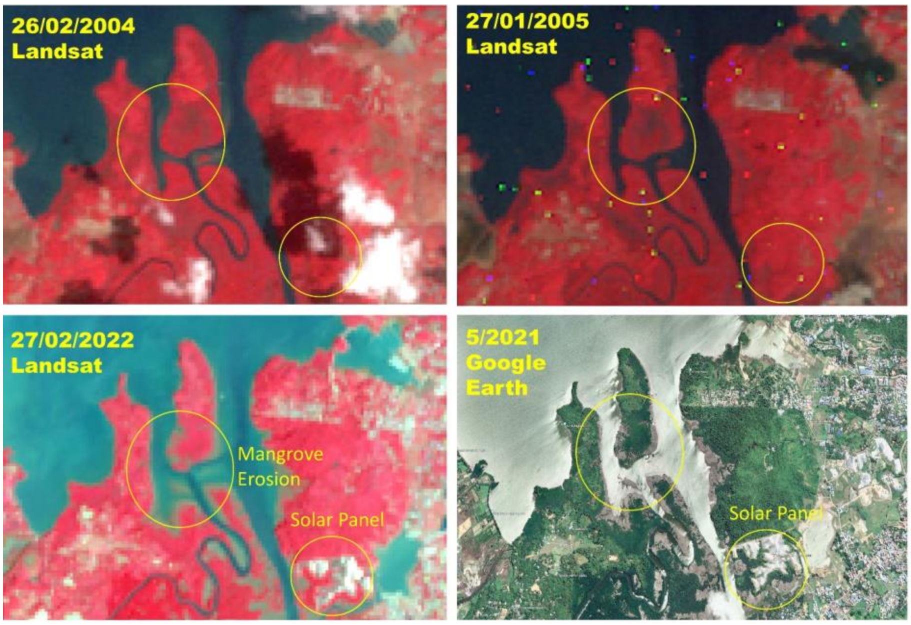

Figure 7: shows a time-lapse satellite imagery of Landsat 8 FCC near the Flat Bay area (marked in yellow circle) during the years 2004 and 2005 showing robust mangrove coverage is evident. However, when comparing the Landsat 8 image in 2022 and the corresponding Google Earth image (@Google Earth), it is apparent that the mangrove ecosystem in this area has experienced substantial erosion and the development of Solar panels.

ZONE 5: The maximum erosion rate of -21.47 m/y (2004-05) and -7.95 (EPR 2005-22) is recorded at Mithakhari. According to the NSM analysis, the shoreline retreated by -19.7 m and -132.39m at Mithakhari (Fig. S8). In this zone, Coastal development, infrastructure construction, and alteration of natural hydrological patterns can disrupt sediment transport and exacerbate erosion (Fig. 8; Table 4).

Deleted: S5

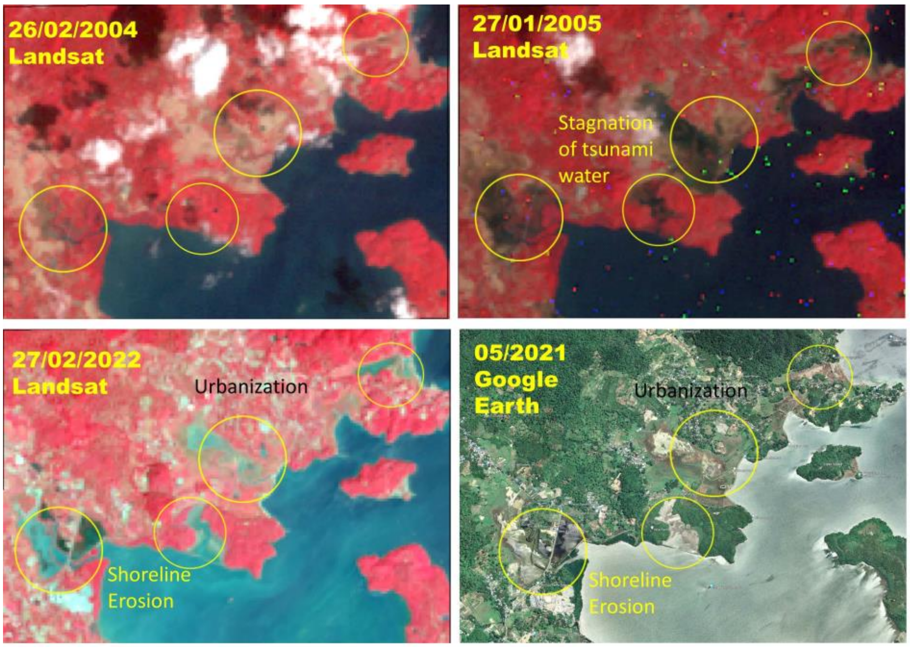

Figure 8: shows Landsat 8 time-lapse imagery and © Google Earth imagery near the Ograbraj and Mithakhari region depicting the erosion activity during and after the tsunami and the imagery shows a significant growth in the built-up areas surrounding the tsunami-affected areas in 2004.

ZONE 6: This zone is predominantly affected by erosion, with no observed accretion. The maximum erosion rate is -21.18 m/y and -7.75 m/y (EPR) at Namunaghar, and the NSM estimated erosion is -19.44 m and -132.39m at Namunaghar (Fig. S9). In February 2004, immediately before the catastrophic tsunami event, there was no observable presence of stagnant water in the area (Fig. 9). However, by January 2005, following the tsunami, the images distinctly exhibited the stagnant water. In February 2022, the same location exhibited substantial shoreline erosion within the extensive mangrove and agricultural area, accompanied by increased urban development along the shoreline. The progression of urban development was also validated using Google satellite imagery. The sediment carried by ocean currents deposited in low-lying areas revealed caused shallowing and significant changes in ocean water color.

Deleted: S6

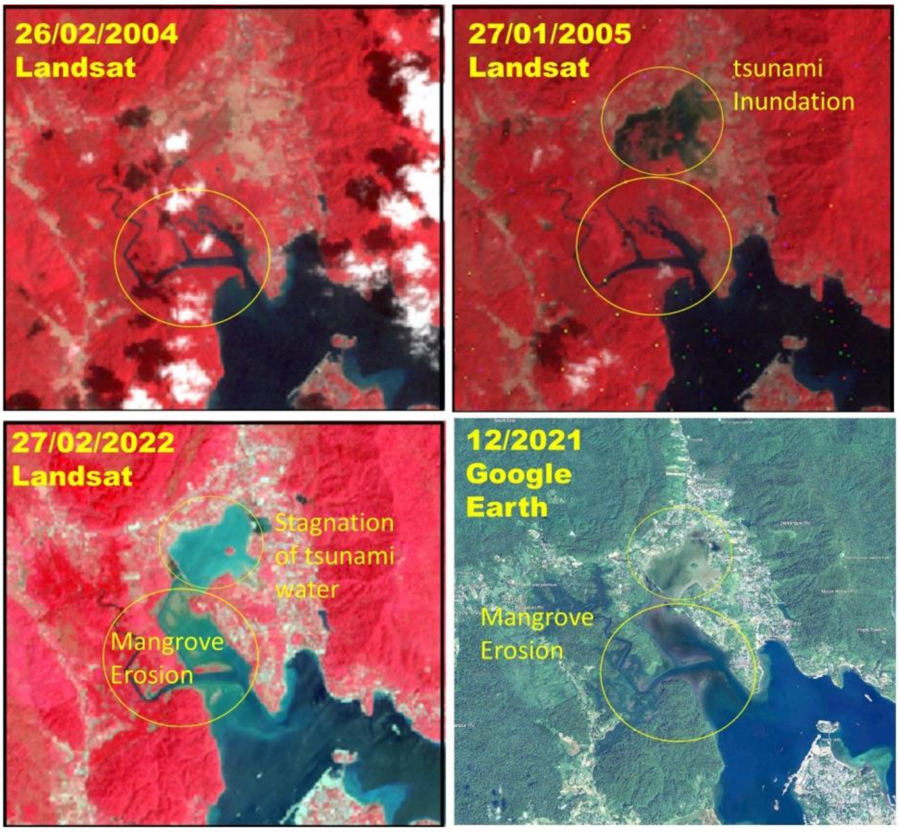

Figure 9: shows the Change detection of the shoreline using Landsat 8 time-lapse imagery and © Google Earth imagery for 2004 before, 2005 after the tsunami, and the 2022 present status of the shoreline.

ZONE 7: This zone experienced a combination of erosion and accretion between 2004-05 and 2005-21. The maximum erosion rate is -8.36 m/y and -11.7 m/y (EPR) at Shore Point, while the maximum accretion rate is 9.77 m/y (EPR). The NSM analysis indicated an erosion of -17.29 m at Shore Point and -199.96 m at North Bay (Fig. S10; Table 4). Notably, a tsunami with a height of 9.6 m was observed at Shore Point.

Deleted: S7

Deleted: is

The natural rate of shoreline movement in the South Andaman region has increased following the tsunami event, which is attributed to several factors, including the removal of vegetation cover, the softening of exposed bedrock, and the destabilization of unconsolidated materials caused by the tsunami, all of which have made the region more susceptible to erosion (Yunus et al., 2016). Comparing the erosion and accretion rates suggests the erosion rates were significantly less during the 2005-2022 period in comparison to the 2004-05 tsunami, highlighting the adverse effect of the tsunami.

4.3 Land Use and Land Cover (LULC) Analysis

The LULC is categorized into 5 distinct classes: Built-up, Forest, Inundation, Cropland, and water Bodies (Fig. 10). The overall accuracy obtained is 90.11%, 89.96%, and 90.30% with a quantitative assessment of K_{hat} (Kappa) coefficient is 0.78, 0.762 and 0.79 for 2004,2005 and 2022 images, respectively (**Table S3**). Our primary objective is to determine the extent of land use pattern changes from 2004 to 2022 in areas affected by the 2004 tsunami. Several researchers have already examined the vulnerability and impact of the 2004 tsunami on South Andaman, including (Velmurugan et al., 2006; Debjani et al., 2012; Sachithanandam,2014).

Deleted: S1

The LULC classification for the South Andaman region in tsunami-impacted areas in the years 2004, 2005, and 2022 reveals significant changes (Fig. 10, Table 5). 1) The built-up area decreased from ~7.38% in 2004 to 6.23% in 2005, marking a 1.15% decrease. However, it subsequently increased by 11.11% by 2022. 2) Cropland coverage decreased from around 22.12% in 2004 to ~11.93% in 2005, indicating a substantial reduction of 10.19%. It then increased to 17.15% by 2022. 3) Inundation areas increased from about 3.29% in 2004 to 27.65% in 2005, showing a notable rise of 24.36%. However, by 2022, they decreased by ~18.57%. 4) Forested areas saw a significant decrease from ~66.46% in 2004 to about 51.10% in 2005, signifying a reduction of 15.36%. This decrease persisted in 2022, remaining at ~51.10%. 5) Water bodies covered around 0.62% of the area in 2004, which increased slightly to about 0.76% in 2005. By 2022, there is a more significant increase, reaching 2.05%.

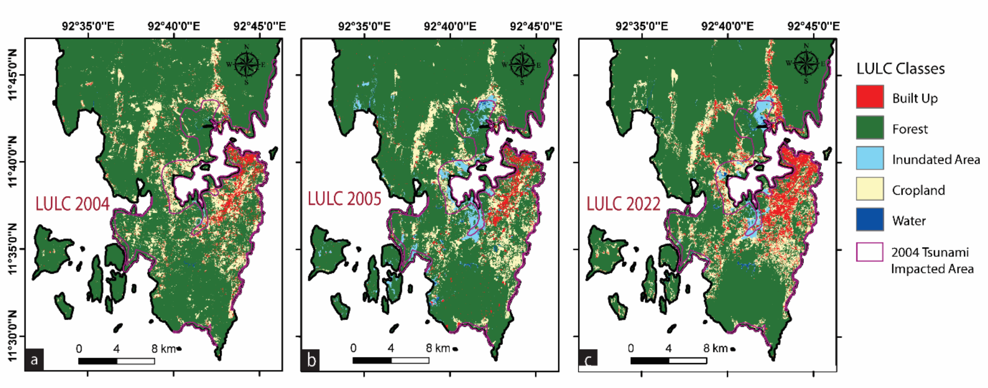

Figure 10: (a) LULC 2004 (b) LULC 2005, and (c) LULC 2022 in tsunami-impacted areas (pink color) and South Andaman.

Table 5: LULC Analysis for 2004, 2005 to 2022 in tsunami impacted area

LULC classes	2004 Area in km^2	2004 % of Area	2005 Area in km^2	2005 % of Area	2022 Area in km^2	2022 % of area
Built-Up	3.57	7.38	3.01	6.23	5.38	11.11
Forest	32.19	66.46	25.79	53.40	24.74	51.10
Inundation Area	1.64	3.39	13.36	27.65	8.99	18.57
Cropland	10.71	22.12	5.76	11.93	24.74	17.15
Water Bodies	0.30	0.62	0.36	0.76	0.99	2.05
Total Area (Sq. Km)	48	100	48	100	48	100

The LULC classification for the South Andaman region in the years 2004, 2005, and 2022 shows significant changes (Figure 10, Table 6)

1) Built-Up Area: In 2004, the built-up area covered 19.92 km², constituting ~3.84% of the total study area. By 2005, this area had reduced to 17.66 km², accounting for 3.41% of the total area. by 2022, there was a significant expansion, with the built-up area occupying 45.07 km², representing 8.68% of the total region.

2) Forest: In 2004, forests dominated the landscape, covering 432.85 km², which was approximately 83.43% of the total study area. By 2005, this forested area slightly decreased to 420.79 km², comprising 81.27% of the total area. However, by 2022, the forest cover continued to decline, with an area of 408.66 km², accounting for 78.78% of the total region.

3) Inundation Area: In 2004, the inundation area was limited, covering 3.40 km² or 0.65% of the total area. In 2005, there was a substantial increase, expanding to 28.41 km², which represented 5.48% of the total area. By 2022, the inundation area decreased to 13.89 km², making up 2.66% of the total region.

4) Cropland: Cropland covered 61.77 km² in 2004, accounting for 11.90% of the total study area. By 2005, this area reduced to 49.34 km², representing 9.53% of the total area. In 2022, the cropland area further decreased to 48.65 km², making up 9.37% of the total region.

5) Water Bodies: In 2004, water bodies covered a small area of 0.83 km², approximately 0.16% of the total area. By 2005, this area slightly increased to 1.54 km², constituting 0.29% of the total region. There was a more significant expansion during 2022, with water bodies occupying 2.45 km², accounting for 0.47% of the total area.

Table 6: LULC Analysis for 2004, 2005 to 2022 in the Study region

LULC	2004 Area in km^2	2004 % of Area	2005 Area in km^2	2005 % of Area	2022 Area in km^2	2022 % of area
Built-Up	19.92	3.84	17.66	3.41	45.07	8.68
Forest	432.85	83.43	420.79	81.27	408.66	78.78
Inundation Area	3.40	0.65	28.41	5.48	13.89	2.66
Cropland	61.77	11.90	49.34	9.53	48.65	9.37
Water Bodies	0.83	0.16	1.54	0.29	2.45	0.47
Total Area (Sq. Km)	518	100	518	100	518	100

5. Discussion

The complex interaction between geomorphology, shoreline change, LULC changes, and economic factors in tsunami vulnerability and impact assessment in South Andaman is discussed below;

5.1 Shoreline changes VS LULC

The impact of tsunamis varies due to differences in landforms, relief, slope, elevation, and the presence (or absence) of natural barriers such as coral reefs and mangroves. It has been observed that for a given water depth on the shelf, if the continental slope is steeper, greater mangrove cover, greater relief, and higher elevation can result in a greater amount of energy being reflected, leading to a smaller tsunami wave height on the shelf. On the other hand, with a flatter slope, low relief, and less vegetation cover area on the coastal side, the reduced reflection and effect of shoaling can increase tsunami wave height (Siva et al., 2016). Coastal erosion is a natural process in south Andaman that occurs when waves, currents, tsunamis, and tides erode the shoreline, removing sediment and land over time. Factors such as sea-level rise, wave energy, storm events, and human activities can contribute to increased rates of erosion.

Over time, the geomorphological landforms continue to shape and modify the landscape. However, human activities and developmental pressures are significant drivers of LULC change in South Andaman (Fig. 10 a, b, c). Common LULC changes observed in the area include deforestation for urban expansion, conversion of land for agriculture, infrastructure development, and alterations to the coastal zone (Yuvaraj et al., 2014; Thakur et al., 2017; Jaman et al., 2022). The interaction between geomorphology and LULC change is particularly evident in the coastal regions of South Andaman, where coastal erosion and accretion processes influence both LULC patterns and development decisions. The erosion occurring near the shoreline leads to the loss of valuable land, affecting agricultural areas and forest regions (Fig. 7,8,9). Conversely, accretion processes can contribute to the growth of coastal areas by building new landforms and influencing land use decisions in those locations (Nagabhatla et al., 2006; Ali and Narayana, 2015; Mageswaran et al., 2021).

5.2 Inundation and run observation

Our computations have shown that the tsunami wave heights for around 5.5 m inundation 90 m are observed in Bombooflat (Fig.4b). Similarly, the harbor area of Port Blair has seen structural failures in some building's foundations, and our computations show wave heights of 3.6m in that area. Chidiya Tapu, which is 25 km from Port Blair, the estimated run-up is 3.9 m, and the inundation is 585 m, which shows a gradual slope in the region (Fig. 2). Coming to the Southpoint Magar area (Port Blair), a high run-up of 8.5 m is computed, and the inundation level is 550 m. Houses located near the open sea were completely washed away. At Wandoor Jetty in Port Blair, the calculated run-up is 3.46, the inundation is 450m, and the saltwater intrusion was observed due to the tsunami.

5.3 LULC vs economic change:

The presence of people, infrastructure, or assets in a hazard-prone location is referred to as exposure, and vulnerability is the degree to which a person, community, or system is susceptible to the impacts of a hazard. Vulnerability is determined by physical, social, economic, and environmental factors. (United Nations Office for Disaster Risk Reduction). Several factors can contribute to changes in exposure, such as population growth, Industrial development, and LULC change. It is anticipated that the population of the Andaman and Nicobar Islands will double by 2050 (Nanda and Haub, 2007), and the islands are experiencing an increasing influx of tourists. The increased population density in these regions intensifies the strain on already vulnerable lands. As a result, when a disaster, such as a natural calamity, occurs in these areas, it affects the tourists and has severe repercussions for the large local population heavily dependent on tourism-related activities (Annan et al., 2005; Wood et al., 2019; Sathiparan et al., 2020, Hamuna et al., 2019). The increases in population from 1971 to 2020, as well as built-up areas, are shown before and after the 2004 tsunami, and GSDP from 2001 to 2020 in tsunami-prone areas of South Andaman are observed in Fig. 11.

Deleted: ¶

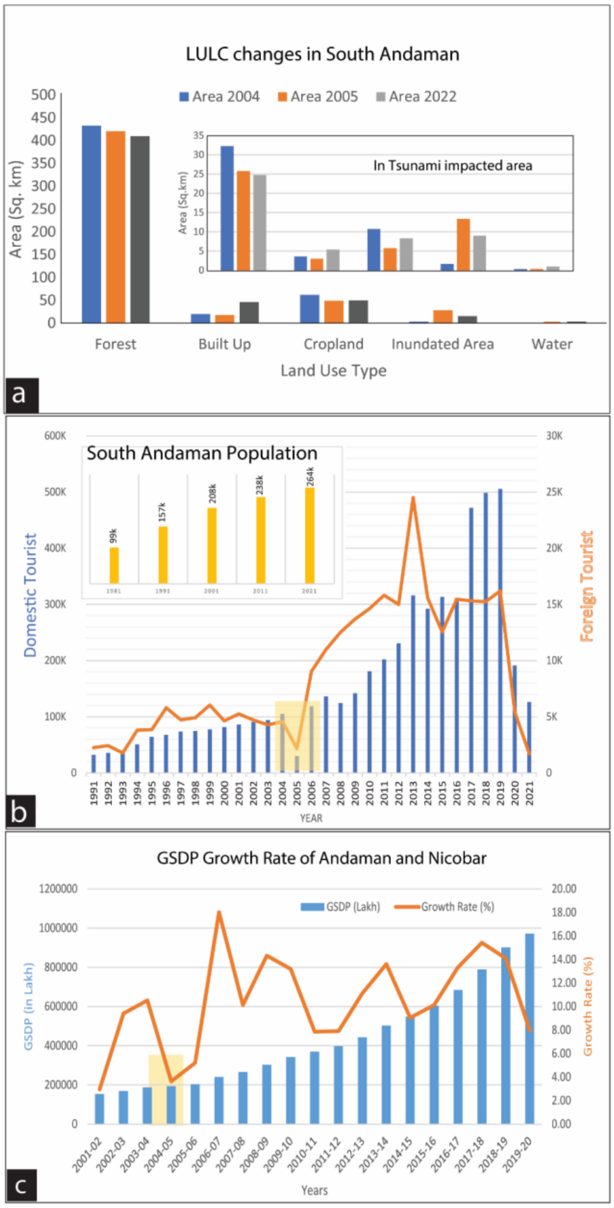

Figure 11: (a) LULC change in south Andaman and also in tsunami-affected areas of 2004. The LULC classification reveals that there has been a significant increase in built-up areas, inundated areas, and water bodies, while the agricultural land and vegetation have decreased. The increasing trends of tourists and local population in south Andaman can be seen in Fig. (b). The GSDP growth rate shows the macroeconomic impact on GSDP in 2005 due to the tsunami impact (c).

The increase in built-up areas could also positively impact the GSDP by boosting the construction and real estate sectors and providing more job opportunities in the tourism and hospitality industries (Fig. 11a). The 2004 Indian Ocean tsunami significantly impacted the GSDP of the Andaman and Nicobar Islands, particularly in the tourism and fisheries industries (Fig 11c). According to a report by the National Institute of Disaster Management, the Andaman and Nicobar Islands suffered losses amounting to INR 7.5 billion due to the 2004 tsunami, with damages to the tourism industry being the most significant. It is important to carefully manage this growth and ensure sustainable development practices protecting both the natural environment and the local population's well-being. This includes implementing effective disaster preparedness measures, promoting sustainable tourism practices, and balancing economic development with environmental conservation in the region.

5.4 Implication for changing scenario of vulnerability

India Inc. estimates that the total losses surpassed Rs 3,000 crore. Specifically, the losses in Andaman & and Nicobar Islands exceeded Rs 1,000 crore as per industry estimates (Economictimes.com). If a tsunami of similar magnitude were to occur again, the economic loss would be five times as high as those experienced in 2004. After the 2004 tsunami, the coastal area experienced significant development, with built-up areas expanding in already affected areas from ~7.38 % in 2004 to ~11.11 % in 2022. This increase in urbanization and infrastructure means that more properties, businesses, and critical facilities are now located in the coastal zone. The affected region's local population grew from 208k in 2001 to 264k in 2021 (Figure 11b). With more people living in the coastal area, there is a higher risk of casualties and a greater demand for resources and aid during and after a tsunami. The number of tourists visiting the coastal area has increased significantly, from 98,000 tourists in 2001 to 500,000 by 2019 (Figure 11b). Tourists are generally less familiar with local hazards and evacuation routes, making them more vulnerable during a tsunami. The presence of a large number of tourists can add complexity to evacuation and relief efforts, potentially leading to higher economic losses. The region has experienced a sharp decline in forest and cropland areas. Forests act as natural buffers, helping to reduce the impact of a tsunami by absorbing some of the wave energy. Additionally, the loss of cropland can disrupt the supply chain during and after a disaster, affecting food availability and leading to economic losses beyond property damage.

6. Conclusions

The South Andaman region is vulnerable to tsunamis due to its location in the seismically active zone. In such an environment, tsunami preparedness and resilience are crucial. This includes implementing effective early warning systems, raising public awareness, and strengthening infrastructure resilience. Incorporating ecosystem-based approaches, such as preserving and restoring natural coastal land, can also contribute to reducing tsunami vulnerability. The South Andaman region is prone to shoreline changes due to natural processes and human activities. Regular monitoring and assessing these changes is crucial to understanding their impacts on coastal ecosystems and communities. Implementing appropriate coastal management strategies, such as beach nourishment, dune restoration, and erosion control measures, can help mitigate the negative effects of shoreline changes. It is important to adopt sustainable land use practices that balance economic development with resource conservation and responsible use. This involves promoting eco-friendly tourism, protecting sensitive ecosystems like mangroves and coral reefs, and implementing land use planning that considers the carrying capacity and vulnerability of the region. Tsunami modeling along the coastal locations shall help decision-makers how to construct structures along the coast. Decision makers will also be able to quantify the tsunami impact on sloping beaches, Flat beaches, and areas having boulders/mangroves. Engaging local communities, stakeholders, and indigenous knowledge holders in decision-making processes and promoting capacity-building initiatives are critical for ensuring the sustainable development of the Andaman region.

Code availability

No

Data availability

All data included in this study are available upon request by contacting the corresponding author**.**

Authors' contributions

Vikas Ghadamode: Computations, Fieldwork, and Manuscript Writing.

K. Kumari Aruna: TUNAMI-N2 Computation and Fieldwork, Manuscript Writing

Anand Kumar Pandey: Manuscript Editing and Contribute Ideas and Suggestions

Kirti Srivastava: Paper Writing and TUNAMI-N2 Computations

Competing interests / Conflicts of interest/

The authors declare that they have no known conflicts of interest.

Declarations

The authors declare that they have no known conflicts of interest.

Financial support

No Funding

Acknowledgements:

The authors acknowledge encouragement and permission to publish from the Director, CSIR-NGRI (Ref. No. NGRI/Lib/2024/Pub-51). VG acknowledges UGC, India, for SRF for pursuing a PhD (Grant no.: 10/UGC-JRF/209/19-ESTT).

References

Ali, P. Y., & Narayana, A. C.: Short-term morphological and shoreline changes at Trinkat Island, Andaman and Nicobar, India, after the 2004 tsunami. Marine Geodesy,38(1), 26-39, https://doi.org/10.1080/01490419.2014.908795 , 2015.

Annan, K.: Reducing Risks from Tsunamis: Disaster and Development. Nueva York: UNDP, 2005.

Bandopadhyay, P. C., & Carter, A.: Chapter 2 Introduction to the geography and geomorphology of the Andaman–Nicobar Islands. Geological Society, London, Memoirs, 47(1), 9-18, https://doi.org/10.1144/M47.2, 2017.

Basheer Ahammed, K. K., & Pandey, A. C.:. Assessment and prediction of shoreline change using multi-temporal satellite data and geostatistics: A case study on the eastern coast of India. Journal of Water and Climate Change, 13(3), 1477-1493, 2022.

Bhat, G.R., Balaji, S. & Yousuf, M.: Tectonic geomorphology and seismic hazard of the east boundary thrust in northern segment of the Sunda–Andaman subduction zone. Nat Hazards 116, 401–423, https://doi.org/10.1007/s11069-022-05680-6, 2023.

Boak EH, Turner IL.: Shoreline definition and detection: a review. J Coast Res 21:688–703, https://doi.org/10.2112/03-0071.1, 2005.

Cho, Y. S., Lakshumanan, C., Choi, B. H., & Ha, T. M.: Observations of run-up and inundation levels from the teletsunami in the Andaman and Nicobar Islands: A field report. Journal of Coastal Research, 24(1), 216-223, https://doi.org/10.2112/06-0662.1, 2008.

Cooper JA, Jackson D, Nava F, McKenna J, Malvarez G.: Storm impacts on an embayed high energy coastline, western Ireland. Marine Geol 210:261–280, https://doi.org/10.1016/j.margeo.2004.05.012, 2004.

Crowell, M., Douglas, B. C., & Leatherman, S. P.: On forecasting future US shoreline positions: a test of algorithms. Journal of Coastal Research, 1245-1255, http://www.jstor.org/stable/4298734, 1997.

Curray, J. R.: Tectonics and history of the Andaman Sea region. Journal of Asian Earth Sciences, 25(1), 187-232, https://doi.org/10.1016/j.jseaes.2004.09.001, 2005.

DANI, B., SRIVASTAVA, V., SINGH, A., & BHATLA, R.; Numerical modeling of tsunami wave to assess the possible impacts along western coasts of India. MAUSAM, 74(4), 1131-1140, 2023.

Dao, M. H., & Tkalich, P., Tsunami propagation modeling–a sensitivity study. Natural Hazards and Earth System Sciences, 7(6), 741-754, 2007.

Davis, R.A.:Human Impact on Coasts. In: Finkl, C.W., Makowski, C. (eds) Encyclopedia of Coastal Science. Encyclopedia of Earth Sciences Series. Springer, Cham, https://doi.org/10.1007/978-3-319-93806-6_175, 2019.

Den Boer, E. L., & Oele, A. C.: Determination of shoreline change along the East-Java coast, using the Digital Shoreline Analysis System. In MATEC Web of Conferences (Vol. 177, p. 01022). EDP Sciences, https://doi.org/10.1051/matecconf/201817701022, 2018.

Devi, E. U., & Shenoi, S. S. C.: Tsunami and the effects on coastal morphology and ecosystems: a report. Proceedings of the Indian National Science Academy, 78(3), 513-521, 2012.

Dolan, R., Fenster, M. S., & Holme, S. J.: Temporal analysis of shoreline recession and accretion. Journal of coastal research, 723-744, http://www.jstor.org/stable/4297888, 1991.

Fletcher, C.H., Romine, B.M., Genz, A.S., Barbee, M.M., Dyer, M., Anderson, T.R., Lim, S.C., Vitousek, S., Bochicchio, C., & Richmond, B.M.: National assessment of shoreline change: Historical shoreline change in the Hawaiian Islands. In (p. 55), 2011.

Ghadamode, V., Srivastava, K., Singh, R. K., & Pandey, A. K.: Spatial analysis techniques for tsunami vulnerability and inundation mapping of Andaman region using remote sensing, GIS, AHP, and Fuzzy logic methods. Environmental Earth Sciences, 81(17), 427, https://doi.org/10.1007/s12665-022-10548-w, 2022.

Ghosh, T., Jana, P., Giritharan, S., Bardhan, S., Basir, S. R., & Roy, A. G.:Tsunami Survey in Andaman Nicobar Group of Islands. *Sumatra–Andaman Earthquake and Tsunami*, *26*, 2004.

Hamuna, B., Kalor, J. D., & Tablaseray, V. E.: The impact of tsunami on mangrove spatial change in the eastern coast of Biak Island, Indonesia. Journal of Ecological Engineering, 20(3), http://dx.doi.org/10.12911/22998993/95094, 2019.

Himmelstoss, E., Henderson, R. E., Kratzmann, M. G., & Farris, A. S.: Digital shoreline analysis system (DSAS) version 5.1 user guide (No. 2021-1091). US Geological Survey, https://doi.org/10.3133/ofr20211091, 2021.

Imamura, F.: Review of Tsunami Simulation with a Finite Difference Method. Long Waves Runup Models, 1996.

Imamura, F., & Imteaz, M. A.: Long waves in two-layers: governing equations and numerical model. Science of Tsunami Hazards, 13(1), 3-24,1995.

Jain, S. K., Murty, C. V. R., Rai, D. C., Malik, J. N., Sheth, A., & Jaiswal, A.: Effects of M9 Sumatra earthquake and tsunami of December 26, 2004. Current Science, 88(3), 357-359, https://www.currentscience.ac.in/Volumes/88/03/0357.pdf, 2005.

Jaman, T., Dharanirajan, K., & Rana, S.: Land use and Land cover Change detection and Its Environmental Impact on South Andaman Island, India using Kappa coefficient Statistical Analysis and Geospatial Techniques, 2022.

Jayakumar K, Malarvannan S.: Assessment of shoreline changes over the Northern Tamil Nadu Coast, South India using WebGIS techniques. J Coast Conserv. 20(6):477–487, https://link.springer.com/article/10.1007/s11852-016-0461-9, 2016.

Jevrejeva, S., Jackson, L., Riva, R., Grinsted, A., & Moore, J.: Sea level rise with warming above 2 degree. In EGU General Assembly Conference Abstracts (p. 3637), 2017.

Joesidawati, M. I.: Shoreline change in Tuban district, East Java using geospatial and digital shoreline analysis system (DSAS) techniques. International Journal of Oceans and Oceanography, 10(2), 235-246, 2016.

Kumar ST, Mahendra RS, Nayak S, Radhakrishnan K, Sahu KC.: Coastal vulnerability assessment for Odisha state, East coast of India. J Coast Res 26:523–534, https://doi.org/10.2112/09-1186.1, 2010.

Kumari P, Jnaneswari K, Rao D, Sridhar D.: Application of remote sensing and geographical information system techniques on geomorphological mapping of coastal part of East Godavari district. Andhra Pradesh, India. Int J Eng Sci Tech 4:4296–4300, https://link.springer.com/article/10.1007/s11069-016-2252, 2012.

Leatherman, S. P.: Shoreline change mapping and management along the US East Coast. Journal of Coastal Research, 5-13, 2003.

Mageswaran, T., Sachithanandam, V., Sridhar, R., Mahapatra, M., Purvaja, R., & Ramesh, R.: Impact of sea level rise and shoreline changes in the tropical island ecosystem of Andaman and Nicobar region, India. Natural Hazards, 109, 1717-1741, https://link.springer.com/article/10.1007/s11069-021-04895-3, 2021.

Mansinha, L., and Smylie, D.E.: The displacements fields of inclined faults, Bull. Seismol. Soci. Am., 61(5), 1433-1440, 1971.

Masaya, R., Suppasri, A., Yamashita, K., Imamura, F., Gouramanis, C., & Leelawat, N.: Investigating beach erosion related with tsunami sediment transport at Phra Thong Island, Thailand, caused by the 2004 Indian Ocean tsunami. Natural Hazards and Earth System Sciences, 20(10), 2823-2841, 2020.

Mishra, P., Usha, T., & Ramanamurthy, M. V.: Evaluation of tsunami vulnerability along the northeast coast of India. Continental Shelf Research, 79, 16-22, 2014.

Misra, A., & Balaji, R.: A study on the shoreline changes and Land-use/land-cover along the South Gujarat coastline. Procedia Engineering, 116, 381-389, https://doi.org/10.1016/j.proeng.2015.08.311, 2015.

Moran CAA.: Spatio-temporal analysis of texas shoreline changes using GIS technique. Mediterranean Mar Sci 2:5–13, https://hdl.handle.net/1969.1/408, 2003.

Mukhopadhyay, A., Mukherjee, S., Hazra, S., & Mitra, D.:Sea level rise and shoreline changes: a geoinformatic appraisal of Chandipur coast, Orissa. *Int J Geol Earth Environ Sci*, *1*(1), 9-17, 2011.

Murali M, Ankitha M, Amritha S, Vethamony P.: Coastal vulnerability of Puducherry coast, India, using analytical hierarchical process. Nat Hazards Earth Syst Sci 13:3291–3311, https://doi.org/10.5194/nhess-13-3291-2013, 2013, 2013.

Murty, C. V. R., Rai, D. C., Jain, S. K., Kaushik, H. B., Mondal, G., & Dash, S. R.; Performance of structures in the Andaman and Nicobar Islands (India) during the December 2004 great Sumatra earthquake and Indian Ocean tsunami. Earthquake spectra, 22(3_suppl), 321-354, 2006.

Nagabhatla, N., Roy, P. S., & Jagdale, R.: Evaluating the change (1968-2001) in landscape pattern and analyzing disturbance in Baratang Forest Division (Andaman Islands), SOUTHEAST ASIA, https://hdl.handle.net/10568/40948, 2006.

Nanda, A. R., & Haub, C.: The future population of India–a long-range demographic view. Popul Res Bureau, 2007.

Natarajan, L., Sivagnanam, N., Usha, T., Chokkalingam, L., Sundar, S., Gowrappan, M., & Roy, P. D.: Shoreline changes over last five decades and predictions for 2030 and 2040: a case study from Cuddalore, southeast coast of India. *Earth Science Informatics*, *14*(3), 1315-1325, 2021.

National Research Council: Tsunami warning and preparedness: an assessment of the US tsunami program and the nation's preparedness efforts, Committee on the Review of the Tsunami Warning and Forecast System and Overview of the Nation's Tsunami Preparedness, National Research Council, 284 pp, 2011.

Nayak S.: Use of coastal data in coastal mapping. Indian Carto CMMC 147–156, 2002.

Raj, N., Rejin Nishkalank, R.A., Chrisben Sam, S.: Coastal Shoreline Changes in Chennai: Environment Impacts and Control Strategies of Southeast Coast, Tamil Nadu. In: Hussain, C. (eds) Handbook of Environmental Materials Management. Springer, Cham. https://doi.org/10.1007/978-3-319-58538-3_223-1, 2020.

Prabhbir Singh., and Kamlesh Khanduri.: Land use and Land cover change detection through Remote Sensing & GIS Technology: Case study of Pathankot and Dhar Kalan Tehsils. Inter. Journal, of. Geomatics and Geosciences 1(4), pp 839-846, 2011.

Prerna, R., Srinivasa Kumar, T., Mahendra, R. S., & Mohanty, P. C.: Assessment of Tsunami Hazard Vulnerability along the coastal environs of Andaman Islands. Natural Hazards, 75, 701-726, https://link.springer.com/article/10.1007/s11069-014-1336-8, 2015.

Ramalanjaona, G.: Impact of 2004 tsunami in the islands of Indian Ocean: Lessons learned. Emergency Medicine International, https://doi.org/10.1155/2011/920813, 2011.

Rani, V. S., Srivastava, K., & Dimri, V. P.: Tsunami propagation and inundation due to tsunamigenic earthquakes in the Sumatra-Andaman subduction zone: Impact at Visakhapatnam. Marine Geodesy, 34(1), 48-58. https://doi.org/10.1080/01490419.2011.547802, 2011.

Reguero, B. G., Beck, M. W., Agostini, V. N., Kramer, P., & Hancock, B., Coral reefs for coastal protection: A new methodological approach and engineering case study in Grenada. Journal of Environmental Management, 210, 146-161, https://doi.org/10.1016/j.jenvman.2018.01.024, 2018.

Rowland, E. D., Lolade, A. A., Nicholas, D. O., Opukumo, A. W., & Omonefe, F.: The Environmental Impact of Shoreline Changes and Land Use/Land Cover Change Detection in the Niger Delta Region using Geospatial Technology. Journal of Asian Scientific Research, 12(4), 237-248, 2022.

Sachithanandam, V., Mageswaran, T., Ragavan, P., Mahapatra, M., Sridhar, R., Ramesh, R., & Mohan, P. M.: Mangrove regeneration in tsunami-affected area of north and south Andaman using insitu and remote sensing techniques, 2014.

Sarkar, D., Mukhopadhyay, A., & Hazra, S.: Nature of tsunami and paleo tsunami deposits of South Andaman. Int J Basic Appl Sci Res, 2(3), 2275-2285, 2012.

Sathiparan, N.: An assessment of building vulnerability to a tsunami in the Galle coastal area, Sri Lanka. Journal of Building Engineering, 27, 100952, https://doi.org/10.1016/j.jobe.2019.100952, 2020.

Scheffers A, Scheffers S, Kelletat D.: Paleotsunami relics on the southern and central Antillean island arc. J Coast Res 21:263–273, https://doi.org/10.2112/03-0144.1, 2005.

Shaw, G., & Williams, A.: Impact of the Tsunami on the Tourism Industry and Ecosystem of the Andaman and Nicobar Islands, India,2006.

Sheth, A., Sanyal, S., Jaiswal, A., & Gandhi, P.: Effects of the December 2004 Indian Ocean tsunami on the Indian mainland. Earthquake spectra, 22(3_suppl), 435-473, https://doi.org/10.1193/1.2208562, 2006.

Singh, A. P., Murty, T. S., Rastogi, B. K., & Yadav, R. B. S.: Earthquake generated tsunami in the Indian Ocean and probable vulnerability assessment for the east coast of India. Marine Geodesy, 35(1), 49-65, https://doi.org/10.1080/01490419.2011.637849,2012.

Siva M.: Behera MR. Effect of continental slope on N-wave type tsunami run-up. The International Journal of Ocean and Climate Systems, https://doi.org/10.1177/1759313116656865, 2016.

South Andaman District – Population.: **https://www.census2011.co.in/census/district/53-south-andaman.html**, 2011-2023.

Srivastava, K., Begum, F., & Jakkula, M.: Tsunami Modelling and Run-ups along Indian Coasts. Journal of the Geological Society of India, 97, 1307-1312, https://doi.org/10.1007/s12594-021-1861-5, 2021.

Sudha Rani NNV, Satyanarayana ANV, Bhaskaran PK.: Coastal vulnerability assessment studies over India: a review. Nat Hazards, https://link.springer.com/article/10.1007/s11069-015-1597, 2015.

Sugawara, D.: Numerical modeling of tsunami: Advances and future challenges after the 2011 Tohoku earthquake and tsunami. Earth-Science Reviews, 214, 103498, 2021.

Thakur, S., Dharanirajan, K., Ghosh, P. B., Das, P., & De, T. K.: Influence of anthropogenic activities on the land use pattern of South Andaman Islands. Research Journal of Marine Sciences, 5(1), 1-10, 2017.

The Economic Times: https://economictimes.indiatimes.com/tsunami-hits-india-inc-with-rs-3000-cr-loss/articleshow/974281.cms?from=mdr

Thieler ER, Himmelstoss EA, Zichichi JL, Ergul A.: Digital shoreline analysis system (DSAS) version 4.0-an ArcGIS extension for calculating shoreline change. US Geological Survey open-file report 2008–1278. US Geological Survey, Woods Hole, https://doi.org/10.3133/ofr20081278, 2009.

Thiéblemont, R., Le Cozannet, G., Rohmer, J., Toimil, A., Álvarez-Cuesta, M., and Losada, I. J.: Deep uncertainties in shoreline change projections: an extra-probabilistic approach applied to sandy beaches, Nat. Hazards Earth Syst. Sci., 21, 2257–2276, https://doi.org/10.5194/nhess-21-2257-2021, 2021

Tonisso H, Suursarr U, Kont A.: Maps, aerial photographs, orthophotos, and GPS data as a source of information to determine shoreline changes, coastal geomorphic processes and their relation to hydrodynamic conditions on Osmussa island, The Baltic sea. IGRSS 12:987–1159, https://doi.org/10.1109/IGARSS.2012.6350382, 2012.

Velmurugan, A., Swarnam, T. P., & Ravisankar, N.: Assessment of tsunami impact in South Andaman using remote sensing and GIS. J. Indian Soc. Remote Sensing, 34(2), 193-202, 2006.

Vu, M. T., Lacroix, Y., & Vu, Q. H.; Assessment of the Shoreline Evolution at the Eastern Giens Tombolo of France. In Proceedings of the International Conference on Innovations for Sustainable and Responsible Mining: ISRM 2020-Volume 2 (pp. 349-372). Springer International Publishing, 2021.

Wood, N., Jones, J. M., Yamazaki, Y., Cheung, K. F., Brown, J., Jones, J. L., & Abdollahian, N.: Population vulnerability to tsunami hazards informed by previous and projected disasters: a case study of American Samoa. Natural Hazards, 95, 505-528, https://link.springer.com/article/10.1007/s11069-018-3493-7, 2019.

United Nations Office for Disaster Risk Reduction (UNDRR): https://www.preventionweb.net/understanding-disaster-risk/component-risk/vulnerability, 2017.

Yunus, A. P., & Narayana, A. C.: Short-term morphological and shoreline changes at Trinkat Island, Andaman and Nicobar, India, after the 2004 tsunami. *Marine Geodesy*, *38*(1), 26-39, https://doi.org/10.1080/01490419.2014.908795, 2015.

Yunus, A. P., Dou, J., Avtar, R., & Narayana, A.: Shoreline and coastal morphological changes induced by the 2004 Indian Ocean tsunami in the Katchal Island, Andaman and Nicobar–a study using archived satellite images. In *Tsunamis and earthquakes in coastal environments* (pp. 65-77). Springer, Cham, https://link.springer.com/chapter/10.1007/978-3-319-28528-3_5, 2016.

Yuvaraj, E., Saravanan, E., & Dharanirajan, K.: Assessment of land use and land cover changes in south Andaman Island using remote sensing and GIS. *Int J Geomat Geosci*, *5*, 171-181, 2014.

Yi, L., Chen, J., Jin, Z., Quan, Y., Han, P., Guan, S., & Jiang, X.: Impacts of human activities on the coastal ecological environment during the rapid urbanization process in Shenzhen, China. Ocean & Coastal Management, 154, 121-132, https://doi.org/10.1016/j.ocecoaman.2018.01.005, 2018.

Zhang, Y., Yin, K., Tang, Y., & Xiao, L.: Tsunami Squares: Leapfrog scheme implementation and benchmark study on wave–shore interaction of solitary waves. Scientific Reports, 14(1), 13053, 2024.

Deleted: coastal management